Retrieval of cloud phase and crystal habit from Multiangle Imaging Spectroradiometer (MISR) and Moderate Resolution Imaging Spectroradiometer (MODIS) data

Sally A. McFarlane, Roger T. Marchand, and Thomas P. Ackerman
Pacific Northwest National Laboratory, Richland, Washington, USA

Received 29 March 2004; revised 4 October 2004; accepted 7 December 2004; published 22 July 2005.

[1] A method of retrieving cloud phase and the dominant ice crystal habit from radiances measured by the Multiangle Imaging Spectroradiometer (MISR) and the Moderate Resolution Imaging Spectroradiometer (MODIS) has been developed. The retrieval method takes advantage of the differences in the phase function of various particle shapes as a function of scattering angle. Three case studies are presented which illustrate the retrieval method. A comparison with semi-coincident in situ observations for one case study indicates that the retrieved crystal habits are consistent with the observations.

Citation: McFarlane, S. A., R. T. Marchand, and T. P. Ackerman (2005), Retrieval of cloud phase and crystal habit from Multiangle Imaging Spectroradiometer (MISR) and Moderate Resolution Imaging Spectroradiometer (MODIS) data, *J. Geophys. Res.*, *110*, D14201, doi:10.1029/2004JD004831.

1. Introduction

[2] Knowledge of cloud phase (liquid or ice) and crystal habit are of fundamental importance to both remote sensing and climate simulations. Using water droplets instead of ice crystals in retrieving cloud properties from satellite data can lead to errors in retrieval of cloud height, optical thickness, and microphysical properties [*Minnis et al.*, 1993; *Mischenko et al.*, 1996]. Satellite retrievals of cirrus cloud microphysical properties are also influenced by the crystal habit used in the retrieval, either indirectly via an assumed phase function or directly via assumed profiles of ice crystal habits [*Nasiri et al.*, 2002]. New methods of retrieving cirrus properties from ground-based remote sensors also depend on particle habit. For example, retrieval algorithms which use radar reflectivity and Doppler velocity measurements to retrieve particle size and ice water content show promise for optically thick cirrus and multilayer cases, which cannot be analyzed with current infrared and lidar methods [*Matrosov et al.*, 2002; *Mace et al.*, 2002]. However, one of the largest uncertainties in radar reflectivity–Doppler velocity retrieval methods is the relationship of fall speed to particle mass, which depends on crystal habit.

[3] In the context of global climate models, the division of cloud condensate between liquid and ice is found to affect the mean climate and climate feedbacks [*Rotstayn et al.*, 2000], but ice crystal habit is also important. Most global climate models currently treat variations in ice particle size and particle shape in simplistic fashion, usually with a fixed particle shape and often with a fixed particle size. Recent work by *Kristjánsson et al.* [2000] using both the National Center for Atmospheric Research (NCAR) Community Climate Model 3 (CCM3) and the United Kingdom Meteorology Office (UKMO) models showed that the treatment of ice particle size and habit are significant, particularly in the tropics. These authors found that the effect of crystal shape and size are of comparable importance to top-of-atmosphere radiative fluxes and that using nonspherical ice crystals warmed the tropical tropopause by an annual average of 1 K, reducing model biases.

[4] Field experiments with in situ aircraft instruments such as the Cloud Particle Imager (CPI) [*Lawson and Blyth*, 1998], which records high-definition digital images of cloud particles, have shown the variability and complexity of crystal habits in cirrus clouds [*Lawson et al.*, 2001; *Fleishauer et al.*, 2002; *Heymsfield et al.*, 2002; *Sassen et al.*, 2003]. While field experiments and in situ observations can provide detailed information about crystal habit and microphysics, they are necessarily quite limited geographically. In order to study the variability of crystal habit on a global scale, remote sensing techniques for retrieving crystal habit from satellite instruments need to be developed.

[5] The shape of a particle affects the scattering of light such that water droplets and ice crystals of various habits have somewhat different phase functions. Consequently the radiances measured by the Multiangle Imaging Spectroradiometer (MISR) instrument aboard NASA's Terra satellite [*Diner et al.*, 2002], which observes light scattered from the same cloud at nine different angles, are functions of the crystal shape. In principle, the measured angular radiance pattern can be used to infer the crystal shape. In recent years, several algorithms have been developed to retrieve crystal habit from satellite data at multiple scattering angles. An examination of radiance measurements from two viewing angles made from the Along Track Scanning Radiometer (ATSR) by *Baran et al.* [1998] has shown the ability to distinguish polycrystals from hexagonal columns and hex-

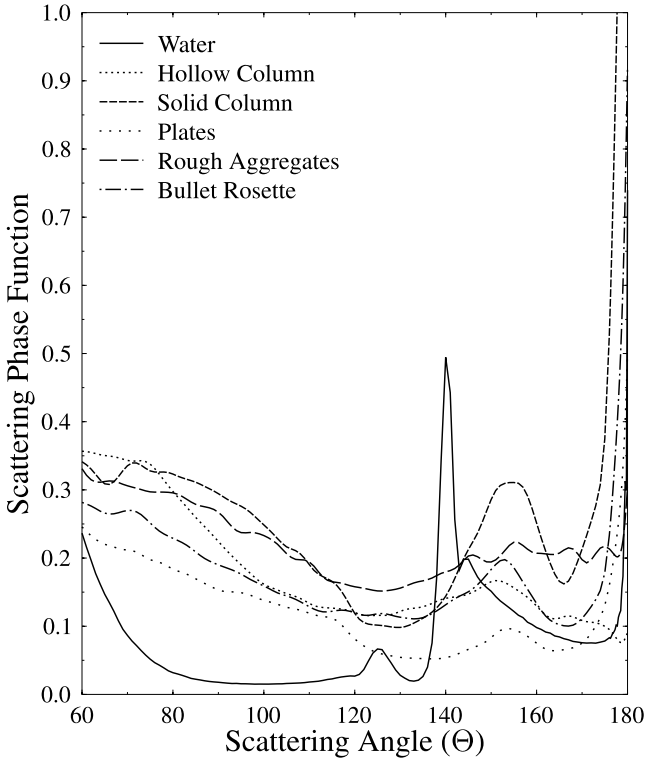

Figure 1. Phase functions calculated for gamma distributions with effective radius of 25 μm for liquid water droplets and various crystal habits.

agonal plates for some tropical cirrus. *Chepfer et al.* [2001] used polarized reflectances measured by the POLarization and Directionality of Earth Reflectance (POLDER) instrument at several scattering angles to retrieve ice crystal shape. They found that polycrystals and columns were common at low latitudes while hexagonal plates were more common at higher latitudes. In these methods, the range of scattering angles viewed in any scene is relatively small, which tends to limit the sensitivity to particle shape. *Chepfer et al.* [2002] developed a method of retrieving crystal habit using visible reflectance from dual satellite measurements, one with viewing angle near the backscatter angle and the other with viewing angle between 60° and 150°. By using two widely separated scattering angles, they found that water clouds could be clearly distinguished from ice clouds and that models containing mixtures of columns, compacts, and bullet rosettes most often matched the data points. No single microphysical model studied was appropriate for all of the cases.

[6] In this paper we present initial results from a cloud phase and ice crystal habit retrieval based on a combination of MISR multiangle measurements in the visible and measurements from the Moderate Resolution Imaging Spectroradiometer (MODIS) instrument in the shortwave infrared. The nine angular measurements provided by the MISR cameras allow a wide range of scattering angles to be viewed in a single scene and should provide reasonable sensitivity to particle habit. The presence of the MODIS instrument on the same satellite allows additional information on particle size to be incorporated into the retrievals. The multiangle approach for cloud phase discrimination described here is considerably different from the current MODIS phase retrieval. A combination of these two approaches will likely be useful for comparison and identification of mixed phase clouds. The crystal habit retrievals could be used to develop regional climatologies of crystal type for use in climate models. Additionally, knowledge of crystal habit will aid in the assessment of and reduction of uncertainties in ground-based and satellite retrievals of cirrus properties in which assumptions about crystal shape are included.

2. Retrieval Algorithm

[7] The MISR instrument, which is described in detail by *Diner et al.* [2002], has nine cameras with view angles of 0° for the nadir camera and 26.1°, 45.6°, 60.0°, and 75.0° for the forward and aft cameras. Each camera obtains images in four narrow spectral bands. The crystal habit retrieval presented in this paper is based on reflectance values from MISR channel 1 (centered at 0.446 μm) due to the low surface reflectance and atmospheric absorption in this channel. The reflectance, R, is calculated for each camera from the MISR Level 1B2 radiance product (version F01) following the equation

$$R = \frac{\pi L d^2}{\mu_0 E_0},$$

where L is the radiance measured by the camera, d is the solar distance in astronomical units, μ_0 is the cosine of the solar zenith angle, and E_0 is the standardized band-weighted solar irradiance for the camera.

[8] The model reflectance for each MISR camera is calculated using the Spherical Harmonics Discrete Ordinates Method (SHDOM) radiative transfer model [*Evans*, 1998] in one-dimensional (1-D) mode. (For the current study, we are comparing the calculated reflectance to averaged MISR observations so only a 1-D radiative transfer calculation is required; in future work we plan to explore the effects of horizontal variability on the retrieval using 2-D radiative transfer). Gaseous absorption is treated with a correlated k-distribution which is based on an absorption spectrum calculated from a line-by-line model and the spectral response function of the instrument. Rayleigh scattering is included in the model, but aerosol effects are neglected. Single scattering properties (phase function, single scattering albedo, and extinction) of ice crystals are obtained from the calculations of *Yang et al.* [2000]. This database provides the single scattering properties of seven different ice crystal habits including columns, plates, aggregates, and bullet rosettes. Bulk scattering properties are obtained by integrating the single scattering properties over a gamma size distribution with shape parameter, α, equal to 1, and a given effective radius and ice water content. The scattering properties of liquid droplets are obtained from calculations based on Mie theory assuming a gamma distribution with $\alpha = 7$.

[9] In Figure 1, phase functions at 0.45 μm are presented for liquid water droplets and several crystal habits for size distributions with an effective radius of 25 um. There are very large differences between the water and ice crystal phase functions, especially for scattering angles between

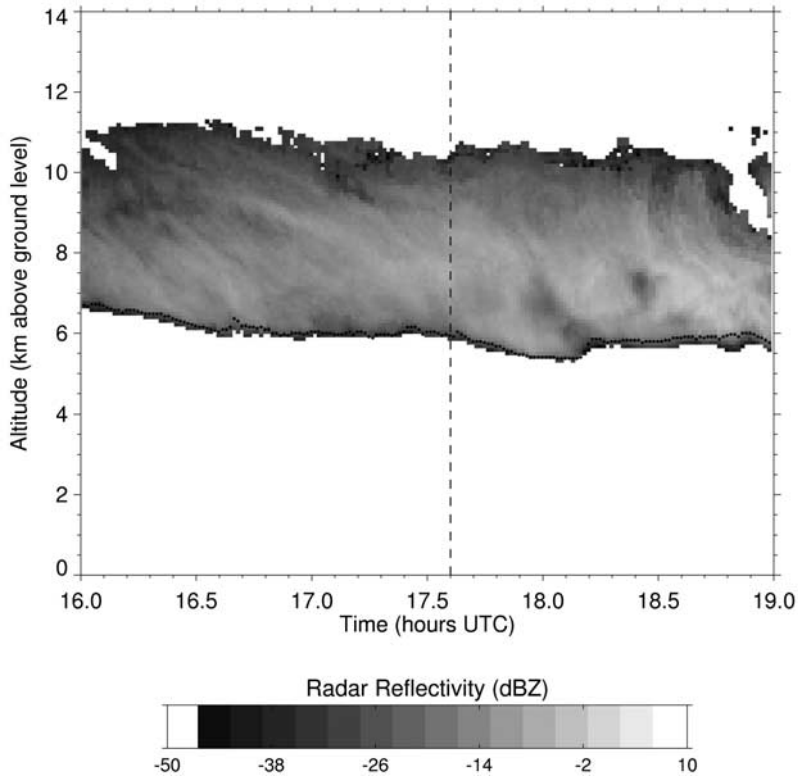

Figure 2. Reflectivity values from the Atmospheric Radiation Measurement (ARM) millimeter wavelength radar for the 6 March 2001 case. The time of the Terra overpass is indicated by the dashed line, and the cloud base derived from micropulse lidar measurements is indicated by the black symbols.

70° and 130°, and near the rainbow feature at 140°. There are smaller but still significant differences in the phase functions of the various crystal habits, especially for scattering angles between 120° and 180°. The basis of the phase and habit retrieval from the MISR angular reflectances is that these differences in the phase function at various scattering angles will translate into differences in reflectance at the MISR viewing angles.

[10] To retrieve particle phase and crystal habit from the MISR reflectances, we assume that the dominant phase or habit will be the one that produces the best match between the MISR observations across all the cameras and the 1-D model calculations. We define a metric, ξ, which is a measure of the mean absolute value of the relative deviation of the modeled and measured reflectances, to assess how well the modeled reflectances match the observations. This metric is given by

$$\xi(\mathrm{R_e}, \mathrm{IWP}, \mathrm{H}) = \frac{1}{\mathrm{N}} \sum_{i=1}^{\mathrm{N}} \left[\frac{|\mathrm{MISR}_i - \mathrm{Mod}_i(\mathrm{R_e}, \mathrm{IWP}, \mathrm{H})|}{\mathrm{MISR}_i} \right],$$

where N is the number of MISR cameras, MISR_i is the observed reflectance from the given camera, Mod_i is the modeled reflectance, R_e is the effective radius, IWP is the ice water path, and H is the crystal habit. The set of R_e, IWP, and H which yields the minimum value of ξ is the retrieved solution. In the current version of the algorithm, each camera is weighted equally in the metric. The minimization is performed by a simple nested minimization scheme using a golden section algorithm.

3. Case Studies

[11] We choose two case studies from Terra overpasses of the Atmospheric Radiation Measurement (ARM) Program's Southern Great Plains (SGP) site in Oklahoma and a third case study from an overpass near the Facility for Atmospheric Remote Sensing (FARS) at the University of Utah in Salt Lake City to demonstrate the algorithm. For the SGP cases, we use the ARM millimeter wavelength radar data to determine the cloud boundaries, while for the FARS case we estimate the cloud boundaries from the polarization diversity lidar (PDL). For each case, we assume a one-layer homogeneous cloud. We average the reflectance for each camera over a 10 km × 10 km box (centered over the ARM site for the SGP cases). For these initial case studies, we ignore the effects of parallax and cloud advection within the MISR observations, although in general these will need to be evaluated carefully.

[12] Where possible, we compare our retrieved cloud properties to other available information, including a ground-based radar retrieval and in situ CPI data for one case. We also compare our retrievals to the MODIS Level 2 (MOD06_L2, version 4.2.5) operational retrievals of cloud phase and optical properties, which are described by *Platnick et al.* [2003]. The MODIS phase retrieval is a bi-spectral algorithm which uses brightness temperature differ-

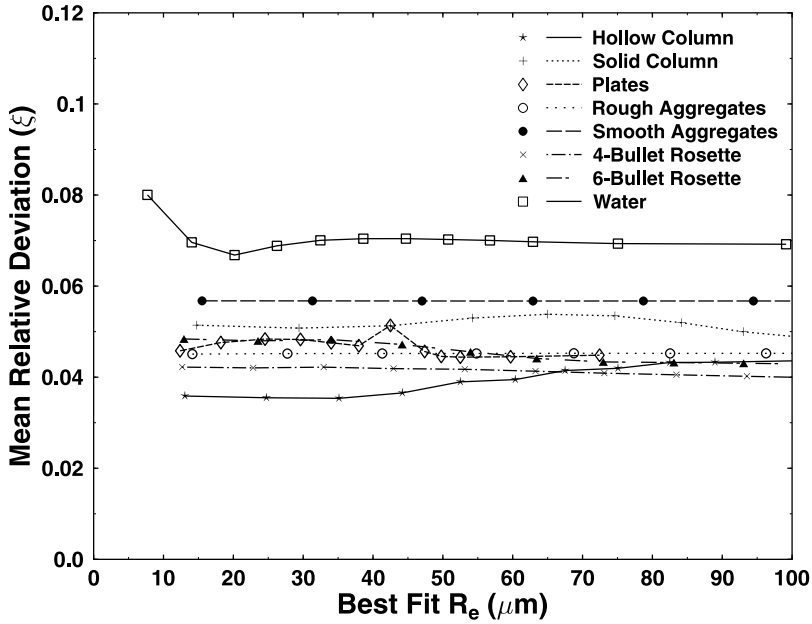

Figure 3. Retrieval metric, ξ, as a function of best fit effective radius for a range of ice water path (IWP) values for the 6 March 2001 cirrus case over the Southern Great Plains (SGP) observed during Multiangle Imaging Spectroradiometer (MISR) orbit 006471. The retrieval is performed using MISR reflectances only.

ences between the 8.52 μm and 11 μm bands to determine cloud phase. The optical retrieval algorithm combines a nonabsorbing band (0.65 μm over land surfaces) with a water-absorbing band at 2.13 μm to retrieve optical depth, effective radius, and water path.

3.1. Cirrus Cloud Case

[13] The first case study is a cirrus cloud that passed over the ARM SGP site on 6 March 2001 (MISR orbit 6471). The ARM millimeter wave radar reflectivity data for this day are shown in Figure 2. The dashed line represents the time of the Terra overpass, and the black symbols represent cloud base derived from micropulse lidar measurements. The cloud base was approximately 6 km and cloud top was near 10.5 km during the Terra overpass. For this case, the solar zenith angle was 44.6° and the MISR scattering angles ranged from 73.6° to 150.6°. Although the radar data indicate that, over a 100 km^2 area centered on the SGP site, the cloud was physically thick, the average optical depth (τ) from the MODIS operational retrievals was only 3.5, with a standard deviation of 0.2 over a 100 km^2 area centered on the SGP site. The MODIS average retrieved effective radius was 29.7 um, with a standard deviation of 1.4 um. The MODIS IR bi-spectral phase retrieval classified the entire cloud as ice.

[14] Figure 3 shows the results of minimizing the mean relative deviation, ξ, between the modeled and measured reflectances for a set of IWP values ranging from 0.005 g m^{-2} to 0.2 g m^{-2}. In this retrieval we use only MISR data. Each point in Figure 3 represents $\xi(R_e)$, where the IWP and the crystal habit are fixed and the value of R_e which yields the smallest possible value of ξ is plotted against that value of ξ. The same range of IWP is used for all the crystal types, and each crystal type is denoted by a different symbol. These results clearly show that water droplets are the worst possible choice to match the MISR reflectance values. This conclusion agrees with the MODIS phase classification. The hollow columns are the best fit to the MISR reflectance values for $R_e < 60$ μm while above 60 μm, several crystal habits appear equally valid. Although smaller particles tend to be favored, in general there is little sensitivity to particle size using only the MISR visible wavelength, in which absorption by ice and water particles is negligible.

[15] To improve the sensitivity of the retrieval to particle size, a near-infrared MODIS channel (Band 7, centered at 2.1 μm) is added to the retrieval algorithm. Owing to absorption by ice and water particles, reflectance in this channel is a strong function of particle size, with reflectance increasing as particle size decreases for a given optical depth. The MODIS standard reflectance product from the 1 km Level 1B calibrated and geolocated files (MOD021KM, version 4.1.2) must be divided by the cosine of the solar zenith angle to make it consistent with the definition given in equation (1). The MODIS Band 7 reflectance is weighted equally with each of the MISR cameras in the retrieval metric. In the top panel of Figure 4 the results of adding the MODIS band to the retrieval are shown. With the addition of the absorbing channel in the near-infrared, the retrievals for each crystal habit now show good sensitivity to particle size. Each particle type shows a clear minimum in the metric, although the best fit effective radius for each type varies greatly. In the bottom panel of Figure 4 the retrieved optical depth as a function of best fit effective radius for the range of IWP is shown. Since the retrieved optical depth is constrained by the MISR nonabsorbing channel, there is little change in the retrieved optical depth with particle size, except for the hexagonal plates.

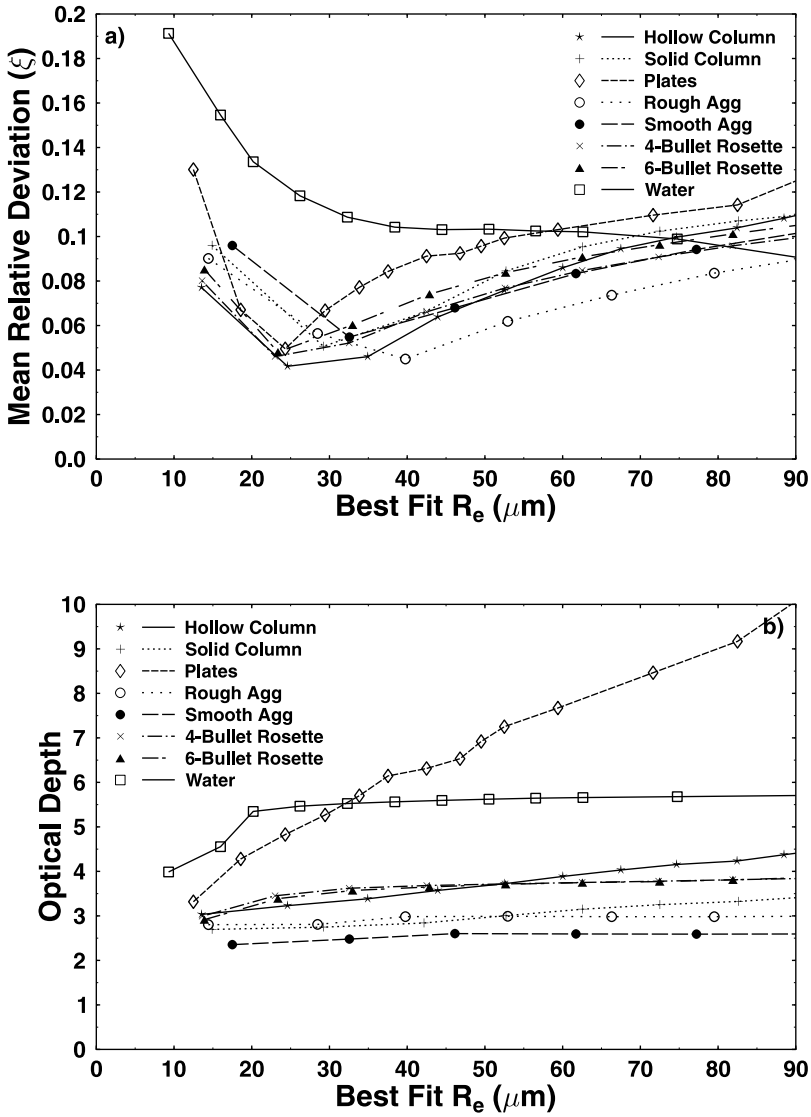

Figure 4. (a) As in Figure 3, but for retrieval based on MISR and Moderate Resolution Imaging Spectroradiometer (MODIS) reflectances. (b) Retrieved optical depth as a function of best fit effective radius for each particle type.

[16] Table 1 presents the results for the full retrieval in which the metric is minimized to solve for R_e and IWP simultaneously. Hollow columns are the best fit, with a retrieved optical depth of 3.3 and effective radius of 27.6 μm, although the metric values are fairly close for all habits except water droplets. The retrieved R_e ranges from 22.5 μm for plates to 37.5 μm for rough aggregates, and the retrieved optical depth ranges from 2.6 for aggregates to 4.8 for plates. The large differences in the retrieved R_e and τ indicate how important it is to use the correct crystal habit in remote sensing retrievals. Also included in Table 1 are the average MODIS operational cloud property retrievals over the 100 km^2 box centered on the SGP site, with the standard deviation over the area given in parentheses. The MOD06 version 4.2.5 retrievals had an error in the coefficient for the calculation of IWP (S. Platnick, personal communication, 2005), so we calculate the MODIS IWP directly from the MOD06 retrieved effective radius and optical depth for each pixel, using the geometrical optics formula IWP = $2/3 R_e \tau \rho_i$,

Table 1. Full Retrieval Results for the 6 March 2001 Cirrus Case[a]

Habit	Metric (ξ)	R_e, μm	IWP, g/m^2	τ
Hollow columns	0.032	27.6	51.3	3.6
Planar rosettes	0.039	27.4	54.5	3.5
Rough aggregates	0.041	37.5	63.5	2.9
Spatial rosettes	0.044	26.1	51.8	3.5
Solid columns	0.046	32.2	49.5	2.8
Hexagonal plates	0.046	22.5	62.1	4.8
Smooth aggregates	0.052	33.8	49.5	2.6
Water droplets	0.09	100	364.1	5.7
MODIS		29.4(1.2)	63.9(1.9)	3.5(0.1)
Radar Retrieval		53.9 (48.1–57.6)	110.3 (82.6–149.5)	3.4 (2.4–5.1)

[a]The effective radius and IWP are retrieved simultaneously by minimizing the metric, ξ. For the MODIS values, the mean and standard deviation over the 10 km × 10 km box are given. The MODIS IWP is calculated from the effective radius and optical depths from the MOD06 product, assuming geometric optics. See text for details of the radar retrieval.

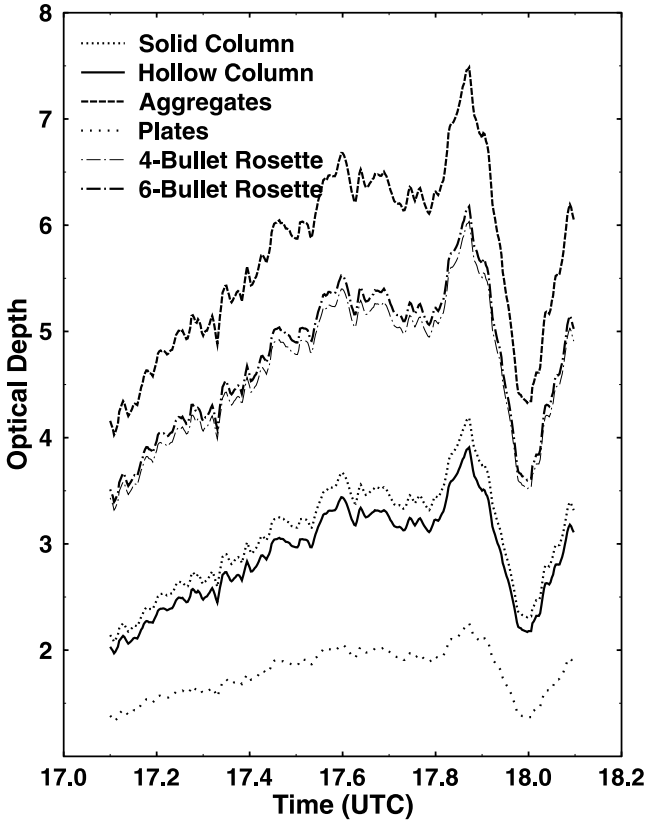

Figure 5. Time series of retrieved optical depth from the radar algorithm as a function of crystal habit.

where ρ_i is the bulk density of ice, 0.92 g/m^3. Our retrieved optical depth and R_e are comparable to the MODIS retrievals, while our retrieved IWP is somewhat smaller.

[17] Since particle fall speed and crystal effective density are strong functions of crystal habit, a primary source of uncertainty in radar retrieval algorithms which use radar reflectivity and Doppler velocity to retrieve vertical profiles of effective radius and ice water content is a lack of knowledge of crystal habit [*Matrosov et al.*, 2002; *Mace et al.*, 2002]. By constraining the particle habit from the MISR retrievals, we can reduce the uncertainty in the radar retrieval results. We use a retrieval algorithm based on work by *Mace et al.* [2002] to retrieve optical depth and effective radius for the 6 March 2001 case. In this algorithm, the first two moments of the Doppler spectrum (radar reflectivity and mean Doppler velocity) are used to retrieve the parameters of the cloud particle size distribution, from which the IWC and effective radius can then be determined. We have made some modifications to the Mace algorithm to ensure that the treatment of particle habit is self-consistent throughout the algorithm. The primary change is that we have replaced the set of three power law relationships used by *Mace et al.* [2002] with a set of equations that all use the same mass and area relationships for a particular ice crystal habit as specified by *Yang et al.* [2000]. Although the power laws used by *Mace et al.* [2002] were each reasonable in isolation, they were all obtained from different sources, so that the treatment of crystal habit throughout the equations was not consistent.

[18] Aside from crystal habit, the other major source of uncertainty in the retrieval algorithm is lack of knowledge of

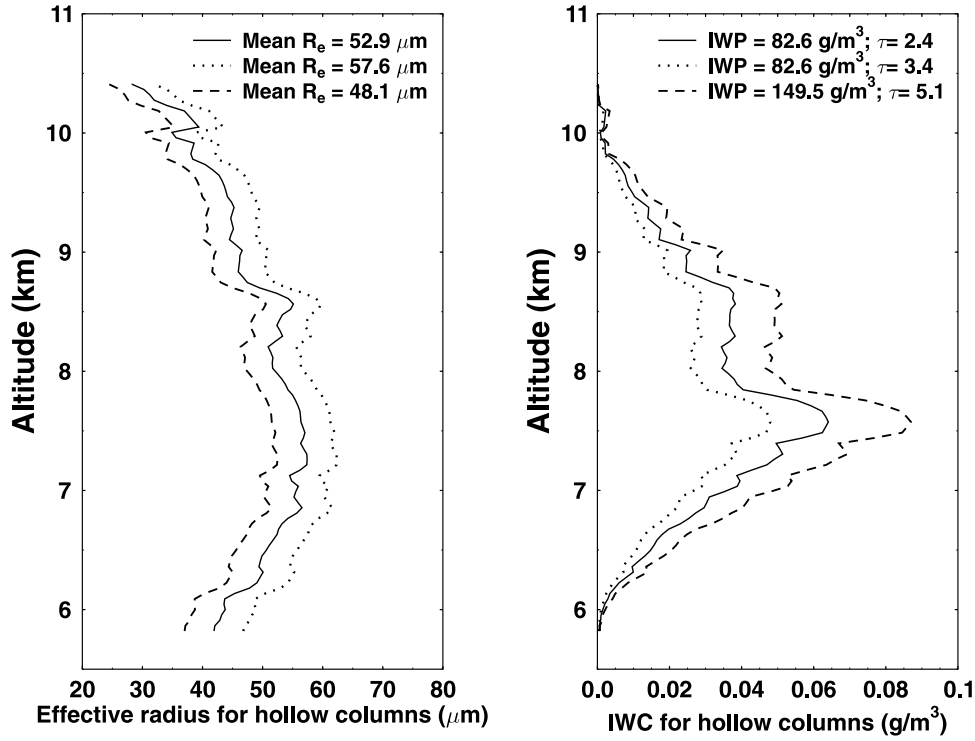

Figure 6. Vertical profiles of (left) retrieved effective radius and (right) ice water content for hollow columns at the time of the Terra overpass. The solid line indicates the retrieval using the best estimate vertical velocity of +10 cm/s, the dotted line indicates the retrieval assuming a vertical velocity of 0 cm/s, and the dashed line assumes a vertical velocity of +20 cm/s.

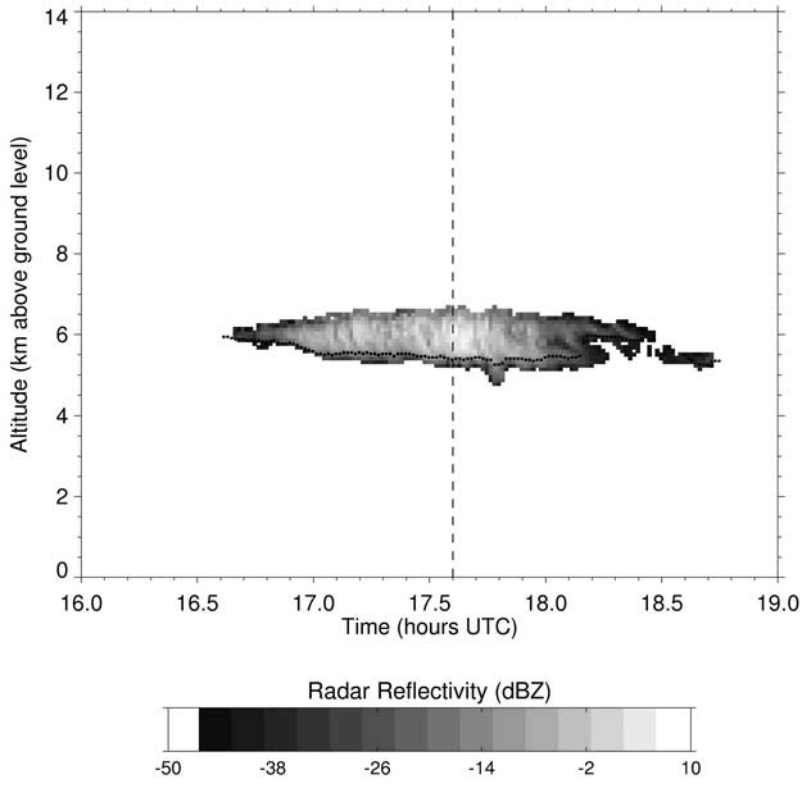

Figure 7. Reflectivity values from the ARM millimeter wavelength radar for the altocumulus case observed over the SGP on 10 June 2001. The time of the Terra overpass is indicated by the dashed line, and the micropulse lidar cloud base is indicated by the black symbols.

the large-scale vertical velocity. Following *Orr and Kropfli* [1998], we used 404-MHz radar wind profiler estimates of vertical velocity in the regions just above and just below the cloud layer to estimate an adjustment to the particle fall speed. This adjustment accounts for mesoscale atmospheric motion which, unlike smaller-scale updrafts and downdrafts, cannot be removed from the cloud radar Doppler velocity by averaging. For this case, the wind profiler data suggest about a 10 cm/s uplift, which we use as our best estimate value.

[19] Figure 5 shows a time series of the retrieved optical depth from the radar algorithm as a function of crystal habit. At the time of the Terra overpass, the retrieved optical depth ranges from 2.0 for plates to 6.7 for aggregates. Knowing that the crystal habit is most likely to be hollow columns constrains the optical depth to a value of 3.4, which is more consistent with the MISR and MODIS retrievals. The retrieved effective radius also depends strongly on crystal habit, with the IWC-weighted mean effective radius varying from 35.0 μm for plates to 57.3 μm for solid columns.

[20] The uncertainty due to crystal habit is slightly larger than the uncertainty due to the vertical velocity assumption. Figure 6 shows the vertical profile of retrieved effective radius and retrieved IWC for hollow columns at the time of the Terra overpass. The solid lines indicate the retrievals using the best estimate vertical velocity of 10 cm/s, while the dotted and dashed lines show the effect of assuming an uncertainty of ±10 cm/s in the vertical velocity. The retrieved IWC weighted mean effective radius ranges from 48.1 μm to 57.6 μm, while the retrieved optical depth ranges from 2.4 to 5.1 with the varying vertical velocity assumptions. The radar retrieved values are listed in Table 1, where the top number represents the value retrieved using hollow columns and the best estimate vertical velocity while the numbers in parentheses represent the range in retrieved values based on the uncertainty in vertical velocity. The radar retrieved optical depth agrees very well with the MISR retrieved values, while the radar effective radius and ice water path are higher. Figure 6 shows that the retrieved particle size from the radar decreases in the top 2 km of the cloud. *Nakajima and King* [1990] showed that the effective radius derived from satellite measurements of reflected solar radiation represents an effective radius at an optical depth of 20–40% of the cloud layer. Thus the satellite retrieved effective radius is more representative of higher levels within the cloud, which may explain the differences in the retrieved effective radius.

3.2. Altocumulus Case

[21] The second case study is a midlevel altocumulus observed over the ARM SGP site on 10 June 2001 (MISR orbit 7869). The ARM millimeter-wave radar data, shown in Figure 7, indicates that cloud base was at roughly 5 km and cloud top was at 6.5 km during the Terra overpass. This mesoscale cloud was actively growing as it passed over the ARM site. The radar also indicated large reflectivity values throughout much of the cloud, which are likely due to large ice crystals to which the millimeter-wave radar is very sensitive. For a 100 km^2 box centered on the SGP site, the mean MODIS retrieved optical depth is 7.9 with a

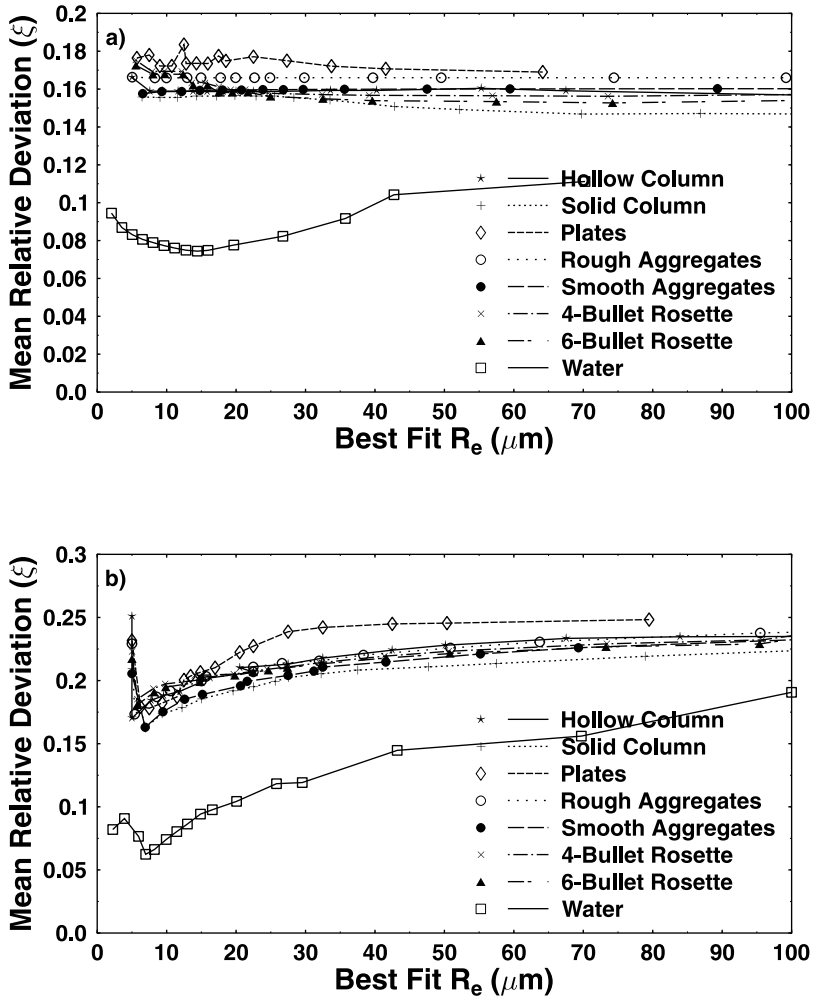

Figure 8. (a) MISR only and (b) MISR and MODIS retrieval results for the altocumulus case observed at the SGP on 10 June 2001 during MISR orbit 007869.

standard deviation of 2.6, the mean retrieved effective radius is 7.9 μm, with a standard deviation of 1.1 μm, and the mean water path is 45.2 with a standard deviation of 12.2 g m^{-2}.

[22] For this case, the solar zenith angle was 18.1° and the MISR scattering angles ranged from 100.1° to 159.7°. Figure 8a shows the best-fit effective radii retrieved using only the MISR reflectance values. The retrieval strongly indicates that liquid water is the preferred phase, with roughly a factor of 2 difference between the minimum deviation for water and the various ice crystal habits. As in the previous case, there is little sensitivity to particle size when only the MISR observations are used. The results of adding the MODIS Band 7 reflectance values to the retrieval are shown in Figure 8b. Again, adding the 2.13 μm absorbing channel gives clear sensitivity to particle size. Assuming liquid water droplets, the retrieved effective radius from the full 2-D retrieval is 7.2 μm, retrieved optical depth is 7.0, and retrieved liquid water path is 31.4 g m^{-2}. These retrievals of R_e and optical depth agree fairly well with the MODIS retrieved values listed above, although the retrieved IWP is smaller than the MODIS value.

[23] The MODIS IR bispectral phase retrieval for this cloud (see Figure 9) indicates that the cloud is primarily ice with a few areas classified as mixed phase and the edges of the cloud mostly classified as water. Although the IR algorithm classified the cloud as primarily ice, the MODIS retrieved particle sizes are relatively small because the

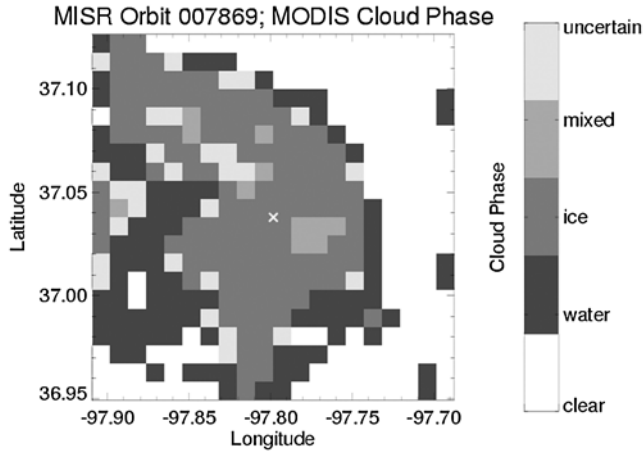

Figure 9. MODIS infrared bispectral phase classification for the altocumulus cloud observed on 10 June 2001. The SGP site is marked by a white cross in the figure.

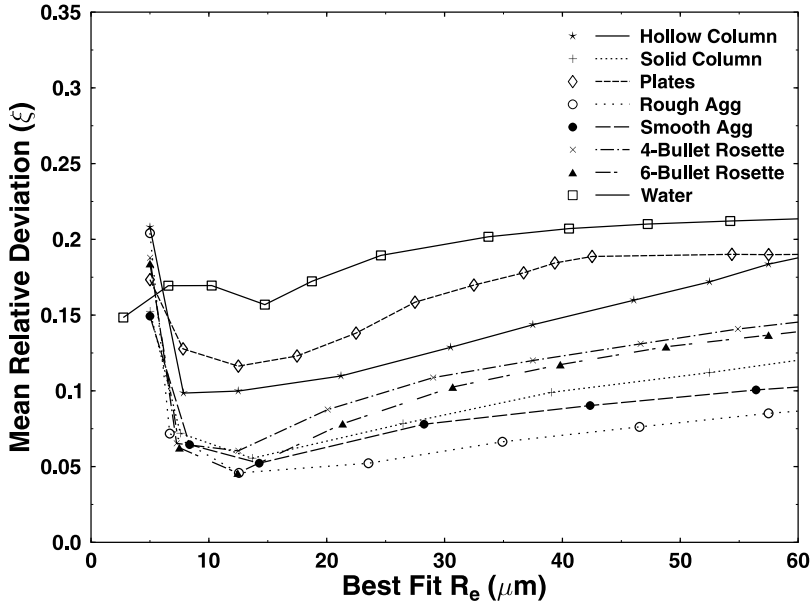

Figure 10. MISR and MODIS retrieval results for the Facility for Atmospheric Remote Sensing (FARS) case observed on 12 November 2001 during MISR orbit 010127.

MODIS cloud microphysical retrievals use their own phase retrieval, based primarily on the reflectance ratios of a shortwave infrared band to a visible band [*Platnick et al.*, 2003]. Given that this cloud was actively growing at the time of the measurements, it is quite plausible that there was liquid water at the top of the cloud. *Fleishauer et al.* [2002] discuss numerous observations that show the tendency of liquid to maximize near cloud top in thin, single-layer mixed clouds in the Arctic, and present similar observations for two cases at the SGP site. Supporting the evidence that the cloud contains liquid, data from the ARM microwave radiometer indicate liquid water paths between 40 and 80 g/m^2 while the cloud was over the ARM site.

[24] Simulations performed by *Chepfer et al.* [2002] indicated that retrieved shape based on visible reflectances at 0.65 μm observed at two different scattering angles was insensitive to multilayer clouds when the optical thickness of the top layer was greater than 2. They concluded that the retrieved shape was only valid for particles within the layer between the top of the cloud and the location where optical depth reached 2. As the retrieved optical depth of this altocumulus cloud was 7.2, the algorithm may detect only the liquid droplets at cloud top and may not be sensitive to ice crystals located lower in the cloud. Combining this retrieval with the MODIS bispectral phase retrieval can improve the detection of mixed phase clouds.

3.3. Case With Semi-Coincident In Situ Data

[25] Currently, there are no cases available at the SGP site in which in situ observations of crystal habit are coincident with a MISR overpass. However, in situ observations were taken by the SPEC Learjet in a cirrus cloud which passed over the FARS site just off the edge of a MISR swath on 12 November 2001. The Polarization Diversity Lidar at the FARS site indicates that the cloud base and top heights were fairly consistent around 9 km and 12 km, respectively, over the period 1830 to 2110 UTC. The aircraft observations were made between 1757 and 2213 UTC at roughly 40.8°N, 112°W. On the basis of radiosondes launched from Salt Lake City at 1200 GMT on 12 November 2001 and 0000 GMT on 13 November 2001, we estimated the wind speed in the cloud layer to be roughly 25 m/s from a southwesterly direction (239°). This agrees well with the wind speed and direction measured by the in situ aircraft, which had mean values of 32 m/s and 224°, respectively, over times when the aircraft altitude was greater than 8 km. The mean wind speed and direction from the MISR stereo height retrieval (version F03) were 26 m/s and 211° over the block. If the wind speed and direction observed by the radiosondes stayed consistent throughout the measurement period, then a fairly homogeneous cloud region observed at 39.6°N, 115°W at 1918 GMT (on the southeastern edge of the MISR swath) would have advected over the FARS site in roughly 3 hours. In this case, the solar zenith angle was 58.0° and there was a very wide range of scattering angles, from 55.1° to 147.9°.

[26] The 1-D retrievals for this case using the MISR and MODIS observations are shown in Figure 10. Again, water is the worst fit solution. The two best fits are rough aggregates and smooth aggregates, followed by solid columns and bullet rosettes. The full 2-D results (listed in Table 2) indicate rough aggregates as the best retrieval with a best fit effective radius of 16.7 μm, optical depth of 2.3, and ice water path of 21.1 g/m^2. In this case, the retrieval metric shows a larger distinction between the different habits than in the first case study. Retrievals from a second fairly homogeneous region of the MISR swath at 40.5°N, 115°W (not shown here) also indicated aggregates as the best retrieval type. The average values of the MODIS retrieval in a 100 km^2 box centered on 39.6°N, 115°W are R_e = 24.2 (3.9) μm, τ = 4.1 (1.5), and corrected IQP = 58.1 (15.4) g/m^2. The MODIS retrieved values or R_e, τ, and IWP

are considerably higher than our retrievals. However, the variability in the MODIS retrievals over the 10 km × 10 km box is also much higher than in the first case study. This indicates that the cloud region is less homogeneous than we assumed, and the MISR retrievals may be affected by the lack of parallax correction.

[27] The MODIS microphysical retrievals assume a size distribution with a mixture of plates, rosettes, and hollow columns when the maximum diameter is <70 μm and a mixture of plates, rosettes, hollow columns, and aggregates when the maximum diameter is >70 μm [*Baum et al.*, 2000]. Images from the Cloud Particle Imager (CPI) on the in situ aircraft show a mixture of crystal habits, with the primary types being aggregates and bullet rosettes. Also seen were a few columns and a region of quasi-spherical small particles near cloud top. No plates were seen in the CPI images. Many of the bullet rosettes were not pristine, but were beginning to melt and aggregate together. Although the in situ observations and the MISR overpass were not coincident so it is not possible to unambiguously match the retrievals with the in situ properties, the habit type retrieved from the algorithm is consistent with the type of crystals detected in the in situ observations. The results in Table 2 show that the largest R_e is retrieved when the ice crystals are assumed to be plates. No plates were observed in the CPI images, and plates are shown to be the worst fit (other than water) to the MISR angular reflectances.

[28] Although the aggregates are not a perfect fit to the observed reflectances, they fit the angular characteristics of the scene better than the other habits, as seen in Figure 11. The inability of the rough aggregates to match the MISR reflectance values at the viewing angles of 26° and 45°, which correspond to scattering angles of 64° and 76.5°, respectively, could be due to a wide range of effects including issues with parallax or cloud advection in the MISR images, variation of the actual crystals from the idealized geometry used in the scattering calculations, or the existence of other habit types within the cloud.

4. Conclusions

[29] We have presented a new retrieval for cloud phase and crystal habit from MISR and MODIS reflectances. The case studies presented here demonstrate that we are able to discriminate cloud phase using the MISR angular measurements alone. Since there is currently no phase retrieval from MISR observations, and this method is considerably different from that used in the MODIS phase retrieval, comparisons between the two methods should be instructive in studying mixed phase or multilayer clouds.

[30] By combining MISR and MODIS measurements, we are able to infer the crystal habit, effective radius, and optical depth simultaneously for ice clouds. The initial tests of the algorithm are quite promising. In the first case study, however, the distinction between the retrieved types was fairly small. Future work involving vertical cloud structure, horizontal variability, corrections for cloud parallax, and investigations of mixtures of particle habits may improve the results. The retrieved values of crystal habit and R_e will in general only be representative of the particles near the top of the cloud. Simulations, as well as comparisons with in situ data, should be performed to determine whether the retrieval is sensitive to vertical structure in the cloud and to what depth within the cloud the retrieved properties are valid.

[31] Comparison to semi-coincident in situ observations indicates that the retrieved habits are reasonable and consistent with the observations. Future cases of coincident in situ observations for validation will greatly help in assessment of the retrieval. The range of effective radius and optical depth retrieved from the observations using different habits shows the strong dependence of retrieved microphysical parameters on assumed habit, which has implications for current retrievals of cirrus properties from satellite data and ground-based radar observations.

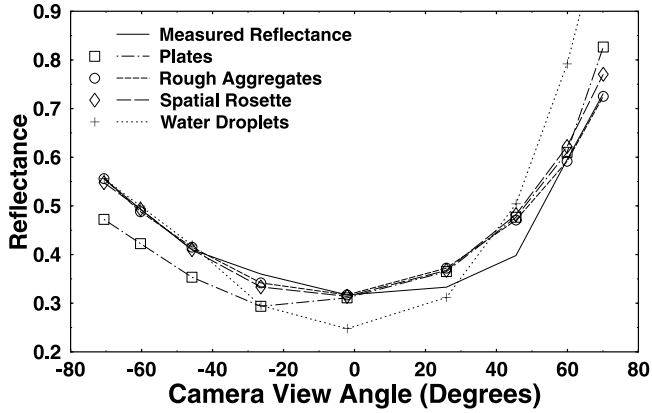

Figure 11. Angular reflectance for the FARS case for the MISR observations and the best fit results for liquid water droplets, rough aggregates, spatial bullet rosettes, and hexagonal plates.

Table 2. Full Retrieval Results for the FARS Case, MISR Orbit 010127[a]

Habit	Metric (ξ)	R_e, μm	IWP, g/m^2	τ
Rough aggregates	0.039	16.7	21.1	2.3
Smooth aggregates	0.053	14.5	15.6	1.8
Solid columns	0.055	14.6	16.8	2.1
Spatial rosettes	0.051	12.8	16.8	2.7
Planar rosettes	0.066	13.1	17.9	2.8
Hollow columns	0.10	13.9	19.1	2.1
Hexagonal plates	0.11	17.5	26.1	3.4
Water droplets	0.16	15.0	31.2	3.6
MODIS		24.2(3.9)	58.1(15.4)	4.1(1.5)

[a]The effective radius and IWP are retrieved simultaneously by minimizing the metric, ξ. For the MODIS values, the mean and standard deviation over the 10 km × 10 km box are given. The MODIS IWP is calculated from the effective radius and optical depths from the MOD06 product, assuming geometric optics.

[32] **Acknowledgments.** The authors thank Ping Yang for providing the ice single scattering properties, Frank Evans for providing the SHDOM radiative transfer code, and Jay Mace for providing the aircraft CPI data. MISR data were obtained from the NASA Langley Distributed Active Archive Center (DAAC).

References

Baran, A. J., P. D. Watts, and J. S. Foot (1998), Potential retrieval of dominating crystal habit and size using radiance data from a dual-view

and multiwavelength instrument: A tropical cirrus anvil case, *J. Geophys. Res.*, *103*, 6075–6082.

Baum, B., D. Kratz, P. Yang, S. Ou, Y. Hu, P. Soulen, and S.-C. Tsay (2000), Remote sensing of cloud properties using MODIS airborne simulator imagery during SUCCESS: I. Data and models, *J. Geophys. Res.*, *105*, 11,767–11,780.

Chepfer, H., P. Goloub, J. Riedi, J. F. D. Haan, J. W. Hovenier, and P. H. Flamant (2001), Ice crystal shapes in cirrus clouds derived from POLDER/ADEOS-1, *J. Geophys. Res.*, *106*, 7955–7966.

Chepfer, H., P. Minnis, D. Young, L. Nguyen, and R. F. Arduini (2002), Estimation of cirrus cloud effective ice crystal shapes using visible reflectances from dual-satellite measurements, *J. Geophys. Res.*, *107*(D23), 4730, doi:10.1029/2000JD000240.

Diner, D. J., J. C. Beckert, G. W. Bothwell, and J. I. Rodriguez (2002), Performance of the MISR instrument during its first 20 months in Earth orbit, *IEEE Trans. Geosci. Remote Sens.*, *40*, 1449–1466.

Evans, K. F. (1998), The spherical harmonics discrete ordinate method for three-dimensional atmospheric radiative transfer, *J. Atmos. Sci.*, *55*, 429–446.

Fleishauer, R., V. Larson, and T. V. Haar (2002), Observed microphysical structure of midlevel, mixed-phase clouds, *J. Atmos. Sci.*, *59*, 1779–1804.

Heymsfield, A., A. Bansemer, P. Field, S. Durden, J. Stith, J. Dye, W. Hall, and C. Grainger (2002), Observations and parameterizations of particle size distributions in deep tropical cirrus and stratiform precipitating clouds: Results from in situ observations in TRMM field campaigns, *J. Atmos. Sci.*, *59*, 3457–3491.

Kristjánsson, J., J. Edwards, and D. Mitchell (2000), Impact of a new scheme for optical properties of ice crystals on climates of two GCMs, *J. Geophys. Res.*, *105*, 10,063–10,079.

Lawson, R. P., and A. M. Blyth (1998), A comparison of optical measurements of liquid water content and drop size distribution in adiabatic regions of Florida cumuli, *Atmos. Res.*, *47–48*, 671–690.

Lawson, R. P., B. A. Baker, C. G. Schmitt, and T. L. Jensen (2001), An overview of microphysical properties of Arctic clouds observed in May and July 1998 during FIRE.ACE, *J. Geophys. Res.*, *106*, 14,989–15,014.

Mace, G. G., A. J. Heymsfield, and M. R. Poellot (2002), On retrieving the microphysical properties of cirrus clouds using the moments of the millimeter-wavelength Doppler spectrum, *J. Geophys. Res.*, *107*(D24), 4815, doi:10.1029/2001JD001308.

Matrosov, S. Y., A. Korolev, and A. J. Heymsfield (2002), Profiling ice mass and characteristic particle size from Doppler radar measurements, *J. Atmos. Oceanic Technol.*, *19*, 1003–1018.

Minnis, P., K. N. Liou, and Y. Takano (1993), Inference fo cirrus cloud properties using satellite-observed visible and infrared radiances: 1. Parameterization of radiance fields, *J. Atmos. Sci.*, *50*, 1279–1304.

Mischenko, M. I., W. B. Rossow, A. Macke, and A. A. Lacis (1996), Sensitivity of cirrus cloud albedo, bidirectional reflectance, and optical thickness retrieval accuracy to ice particle shape, *J. Geophys. Res.*, *101*, 16,973–16,985.

Nakajima, T., and M. D. King (1990), Determination of the optical thickness and effective particle radius of clouds from reflected solar radiation measurements: Part I. Theory, *J. Atmos. Sci.*, *47*, 1878–1893.

Nasiri, S. L., B. Baum, A. J. Heymsfield, P. Yang, M. R. Poellot, D. P. Kratz, and Y. Hu (2002), The development of midlatitude cirrus models for MODIS using FIRE-I, FIRE-II, and ARM in situ data, *J. Appl. Meteorol.*, *41*, 197–217.

Orr, B. W., and R. A. Kropfli (1998), A method for estimating particle fall velocities from vertically pointing Doppler radar, *J. Atmos. Oceanic Technol.*, *16*, 29–37.

Platnick, S., M. D. King, S. A. Ackerman, W. P. Menzel, B. A. Baum, J. C. Riedi, and R. A. Frey (2003), The MODIS cloud products: Algorithms and examples from Terra, *IEEE Trans. Geosci. Remote Sens.*, *41*, 459–473.

Rotstayn, L., B. Ryan, and J. Katzfey (2000), A scheme for calculation of the liquid fraction in mixed-phase stratiform clouds in large-scale models, *Mon. Weather Rev.*, *128*, 1070–1088.

Sassen, K., W. Arnott, D. O. Starr, G. Mace, Z. Wang, and M. Poellot (2003), Midlatitude cirrus clouds derived from Hurricane Nora: A case study with implications for ice crystal nucleation and shape, *J. Atmos. Sci.*, *60*, 873–891.

Yang, P., K. N. Liou, K. Wyser, and D. Mitchell (2000), Parameterization of the scattering and absorption properties of individual ice crystals, *J. Geophys. Res.*, *105*, 4699–4718.

T. P. Ackerman, R. T. Marchand, and S. A. McFarlane, Climate Physics Group, Pacific Northwest National Laboratory, P.O. Box 999, MS K9-24, Richland, WA 99352, USA. (sally.mcfarlane@pnl.gov)